Biogeosciences, 10, 7293–7306, 2013
www.biogeosciences.net/10/7293/2013/
doi:10.5194/bg-10-7293-2013

On the role of mesoscale eddies for the biological productivity and biogeochemistry in the eastern tropical Pacific Ocean off Peru

L. Stramma[1], H. W. Bange[1], R. Czeschel[1], A. Lorenzo[2], and M. Frank[3]

[1]Helmholtz Centre for Ocean Research Kiel (GEOMAR), Düsternbrooker Weg 20, 24105 Kiel, Germany
[2]Instituto del Mar del Peru (IMARPE), Coastal Laboratory of Pisco, Paracas-Pisco, Peru
[3]Helmholtz Centre for Ocean Research Kiel (GEOMAR), Wischhofstraße 1–3, 24148 Kiel, Germany

Correspondence to: L. Stramma (lstramma@geomar.de)

Received: 22 May 2013 – Published in Biogeosciences Discuss.: 10 June 2013
Revised: 11 October 2013 – Accepted: 13 October 2013 – Published: 14 November 2013

Abstract. Mesoscale eddies seem to play an important role for both the hydrography and biogeochemistry of the eastern tropical Pacific Ocean (ETSP) off Peru. However, detailed surveys of these eddies are not available, which has so far hampered an in depth understanding of their implications for nutrient distribution and biological productivity. In this study, three eddies along a section at 16°45′ S have been surveyed intensively during R/V *Meteor cruise M90* in November 2012. A coastal mode water eddy, an open ocean mode water eddy and an open ocean cyclonic eddy have been identified and sampled in order to determine both their hydrographic properties and their influence on the biogeochemical setting of the ETSP. In the thermocline the temperature of the coastal anticyclonic eddy was up to 2 °C warmer, 0.2 more saline and the swirl velocity was up to 35 cm s^{-1}. The observed temperature and salinity anomalies, as well as swirl velocities of both types of eddies were about twice as large as had been described for the mean eddies in the ETSP. The observed b248(te6(of)-nic)-2 r0y12.-nicas13(r0ye)1(2.1(2.1(0e,--272(ASA)-250(10)--272(as13(r0ye)1(2.1(9s13(r0ye)1(2.1(r

euphotic zone, primarily at fronts (Mahadevan and Archer, 2000). Thus, cyclonic eddies (cyclones) and mode water eddies can inject nutrients from below the euphotic zone into the euphotic zone while anticyclonic eddies (anticyclones) tend to decrease the nutrient content of the euphotic zone (e.g. Klein and Lapeyre, 2009). The enhanced upwelling of

maximum upwelling (in austral winter) and satellite observation of the maximum chlorophyll concentrations (in austral summer) in the coastal area of Peru may be caused by an intensification and seasonal displacement of eddy kinetic energy associated with eddies north of 20° S. Moreover, coastal eddies off Peru have been shown to be sites of significant loss of fixed nitrogen (Altabet et al., 2012). Therefore, eddies off Peru seem to play an important role for biological productivity and the nitrogen cycle. However, our knowledge is mainly based on model studies and satellite observations but actual (i.e. in-situ) hydrographic and biogeochemical features of the eddies off Peru are largely unknown. Here we present the results of a first detailed survey of hydrographic and biogeochemical parameters of three eddies off Peru in order to elucidate their role for the biogeochemical cycling in the ETSP.

2 Observational data

Cruise M90 on the German research vessel R/V *Meteor* took place in November 2012 to investigate the factors controlling the intensity and areal extent of the OMZ of the eastern tropical Pacific Ocean. The cruise started in Cristobal, Panama, on 29 October and ended on 28 November in Callao, Peru. Starting on 15 November a former World Ocean Circulation Experiment (WOCE) section along 16°45 S sampled in April 1994 was reoccupied by following an eastward cruise track from 87° W to the coast of Peru. On the basis of satellite sea level height anomaly images forwarded to the ship and which revealed two major anticyclonic eddies and one cyclonic eddy along the section (Fig. 1), a detailed survey of these eddies including acoustic Doppler current profiling (ADCP), measurements of conductivity/temperature/depth (CTD), and of major biogeochemical parameters (O_2, nutrients, chlorophyll, turbidity and pH) along several additional subsections across the eddies have been performed (Fig. 1). The surveys were carried out on 16 to 18 November for section B, on 20 and 21 November for section C, on 22 and 23 November for section A2 and on 24 and 25 November for section A1.

Two ADCP systems recorded the ocean velocities: a hull mounted RDI OceanSurveyor 75 kHz ADCP provided the velocity distribution to about 700 m depth, while a 38 kHz ADCP mounted in the sea-well provided velocity profiles down to about 1200 m depth. Given that the eddies are centred in the upper ocean the data shown in this study for the upper ocean are exclusively from the 75 kHz ADCP, which has a higher resolution in the upper ocean. The 38 kHz ADCP data are used to determine the swirl velocities below 700 m depth.

A Seabird CTD system with a GO rosette with 24 10 L-water bottles was used for water profiling and discrete water sampling. The CTD system was used with double sensors for temperature, conductivity (salinity) and oxygen. The CTD oxygen sensor was calibrated with oxygen mea-

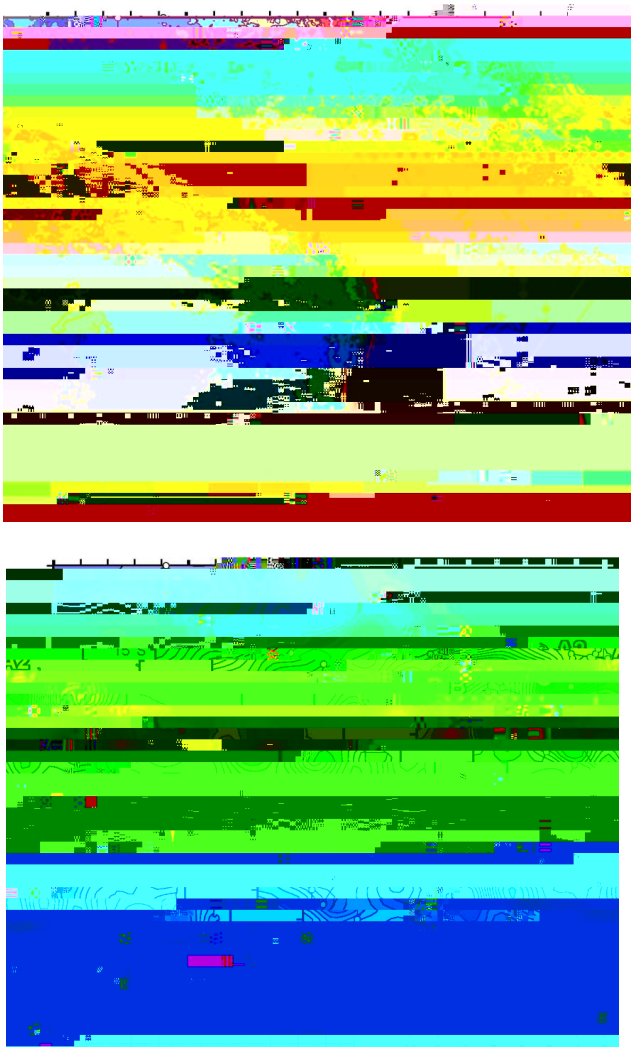

Fig. 1. Mean monthly November 2002 to 2011 chlorophyll data binned spatially and temporally over the entire month with the 200 m and 2000 m depth contours included as white lines (top) and Aviso sea level height anomaly (in cm) for 21 November 2012 (bottom), cyclonic features are shown in blue, anticyclonic ones in red.

chlorophyll concentrations ($\mu g\,L^{-1}$) were measured with a WetLabs FLNTU instrument attached to the CTD. We used the original calibration provided by the company with sensitivities of 0.01 NTU and $0.025\,\mu g\,L^{-1}$ but did not apply any shipboard calibration and hence the measured absolute values may have a somewhat larger uncertainty, but the gradients determined across the eddies are clearly reliable. As the chlorophyll data are only company calibrated we will mark the units as (cc)$\mu g\,L^{-1}$.

Nutrients were measured on-board with a QuAAtro auto-analyser (Seal Analytical). Nitrite (NO_2^-), nitrate (NO_3^-), phosphate (PO_4^{3-}) and silicate (SiO_2) were measured with a precision of $\pm 0.1\,\mu mol\,L^{-1}$, $\pm 0.1\,\mu mol\,L^{-1}$, $\pm 0.02\,\mu mol\,L^{-1}$ and $\pm 0.24\,\mu mol\,L^{-1}$, respectively. N* was calculated as $N^* = (NO_3^- + NO_2^-) - 16\,PO_4^{3-}$ (see Altabet et al. (2012) and references therein).

The pH measurements were carried out with a Mettler Toledo potentiometer, model SevenGo, with an InLab 413 SG IP67 electrode calibrated with buffer solutions at pH values 4, 7 and 10.

Eddy core anomalies were calculated as the difference between concentrations measured at the stations at the edge of the eddy and those in its centre. As we can only use stations available from our measurements, the definition of the eddy core and the eddy boundary might differ to the real eddy core and boundary. The locations chosen for comparison are marked in the figures representing each section. The available heat anomalies (AHA) and available salt anomalies (ASA) were computed as described in Chaigneau et al. (2011). For AHA and ASA the maximum of swirl velocity from the ADCP was defined on both sides of the eddy for each depth and then temperature and salinity were interpolated on an equidistant grid between these boundaries from all existing profiles along the section and the gridded field was used for the AHA and ASA computation.

Aviso satellite derived altimeter sea surface height anomaly data (SSHA) were used to define the general distribution of eddies and to identify their individual spatial extent during the cruise and their generation and path in time. The SSHA data used in this study are delayed time products and combine available data of all satellites. The data are resampled on a regular $0.25^\circ \times 0.25^\circ$ grid and are calculated with respect to a seven-year mean (http://www.aviso.oceanobs.com). For the overview figure (Fig. 1b) the delayed time 7 day mean SSHA image was used, while for tracking the eddy movement the daily final near real time products were used. The eddies were tracked for each day and for selected days the centre was taken at the location of the largest SSHA deviation. MODIS-aqua satellite derived chlorophyll data were used for a better visualisation of the distribution of chlorophyll at the surface of the coastal eddy. The chlorophyll data provided by the Giovanni data portal (http://disc.sci.gsfc.nasa.gov/giovanni/additional/users-manual) are either a monthly mean image for all November data 2002 to 2011 (Fig. 1a) or averaged for each grid cell over a time range of 8 days with a resolution of $1/24^\circ \times 1/24^\circ$.

The focus of the investigation is on the measured parameters hence the eddy boundaries are defined from the measured profiles together with the high resolution ADCP data. Using the satellite data to define the boundaries might result in locations not measured. The satellite data derived with interpolation schemes from available satellite paths do not represent the subsurface parameter distribution in the eddy.

3 Results

3.1 Eddies off southern Peru

Several anticyclonic (counter-clockwise rotation in the Southern Hemisphere) and cyclonic features were clearly visible in the SSHA data in the region off Peru at the time of cruise M90 in November 2012 (Fig. 1b). Along the $16^\circ 45'$ S section one anticyclonic eddy (eddy B) was centred in the open ocean at about 17° S, $83^\circ 30'$ W and another anticy-

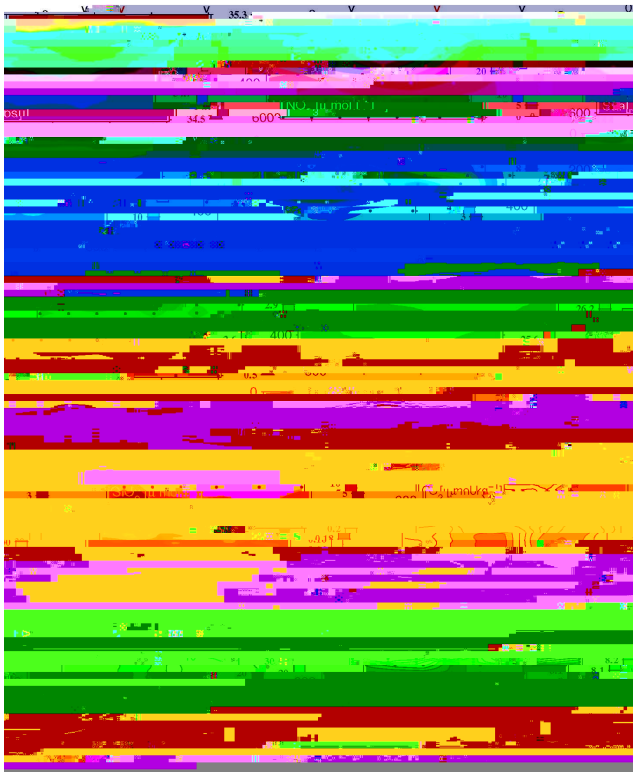

Fig. 2. Parameter distribution in the anticyclonic eddy A off the Peruvian shelf along section A1 from 15° 10′ S, 76° 42′ W to 17° 30′ S, 76° W (see Fig. 1) on 24 and 25 November 2012 for salinity, temperature, density, oxygen concentrations and zonal (u, positive eastward) and meridional (v, positive northward) ADCP velocity components (left), nitrate, nitrite, phosphate, silicate concentrations, turbidity and pH (right). For bottle data of the nutrient concentrations and pH the sampling depths are marked by black dots. To compute the eddy core anomalies in Fig. 3, the two outside profiles used are marked on top with a black v and the core profile with a red v.

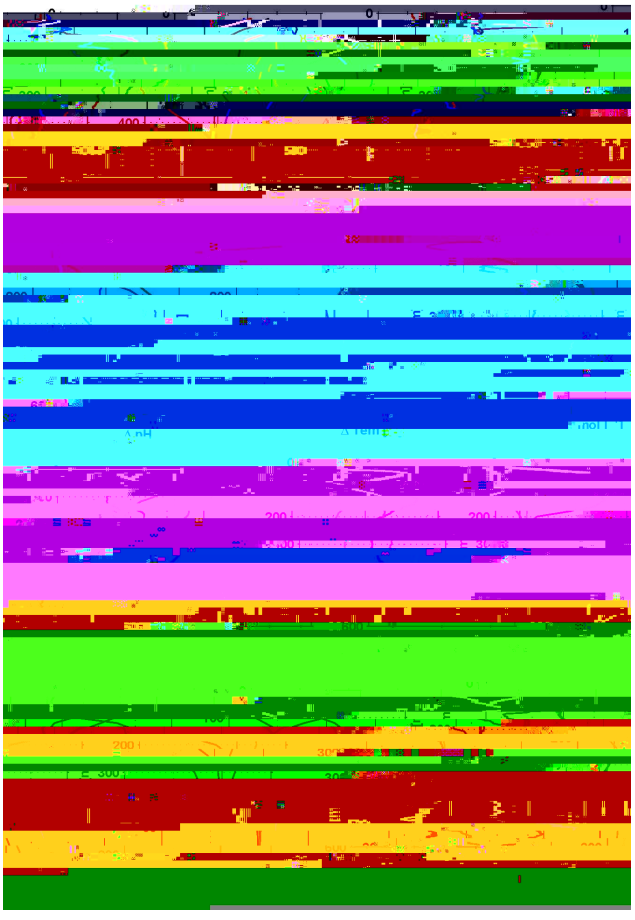

Fig. 3. Eddy core anomalies from the difference between the mean of the two profiles outside the eddy and in the profile in the eddy core (as marked by red and black v's in the section plots) versus depth for salinity, temperature, density and oxygen concentration (left), nitrate, nitrite, phosphate, and silicate concentration (middle), turbidity, pH, swirl velocity and N^2 (right) for the near-shelf anticyclonic eddy A (see Fig. 2) between 76.6° W and 76° W (red lines), the open ocean anticyclonic eddy B (see Fig. 7) between 85° 30′ W and 82° 30′ W (black lines) and the cyclonic eddy C (see Fig. 8) between 15° S and 17.5° S (blue lines). For oxygen the x axis is changed at 300 m depth to better resolve the small changes at depth.

minimum linked to the eddy is clearly visible in the section across the eddy (Fig. 2). There is a pronounced decrease of the oxygen concentrations by more than 200 µmol kg^{-1} from the surface to 50 m depth (Fig. 3) where the uplift of the near surface isopycnals led to a significant shoaling of the mixed layer. Nitrate was reduced at 100–300 m depth by □ 20 µmol L^{-1} and nitrite increased at 100–500 m depth. A pronounced increase in phosphate and silicate concentration was observed between 50 m and 150 m depth. Turbidity was higher at about 50–400 m depth and the pH was generally higher between 100 m and 400 m depth, but displayed the highest decreasing gradient from the surface down to around 50 m depth (Fig. 3). The chlorophyll distribution in the upper ocean was characterised by a very large chlorophyll maximum of 6.1 (cc)µg L^{-1} in the core of uprising isopycnals at 45 m to 55 m depth for the centre of the anticyclone (Fig. 4) connected to a positive turbidity anomaly of 0.1 NTU (Fig. 3). The increased chlorophyll values near the surface at 76.6° W to 76.7° W were related to high near coastal chlorophyll values, which were visible in chlorophyll satellite images taken at the end of November 2012 (Fig. 5) and which were transported offshore at the northern rim of the anticyclone. While the mean November surface chlorophyll distribution shows a large high chlorophyll layer reaching off the shelf-break (Fig. 1a), the surface chlorophyll is strongly reduced in mid-November 2012 in the area of the eddy A flow component towards the shelf (Fig. 5).

According to sea level anomaly images this anticyclone was formed after 13 September 2012. It appeared first on 14 September 2012 at 16° 15′ S 75° W. It moved to 16° 15′ S, 76° W on 1 November 2012 with a mean westward velocity

Fig. 6. Parameter distribution in the anticyclonic eddy A, section A2 off the Peruvian shelf from 77° W, 16°45′ S to 76° W along 16°45′ S and then northeastward to 75°09′ W, 15°30′ S (see Fig. 1) on 22 and 23 November 2012 for salinity, temperature, density, oxygen concentrations and zonal (u, positive eastward) and meridional (v, positive northward) ADCP velocity components (left) and the eastern part of section A2 only (east of the dashed line in the left frames) as no bottle data were collected between 76° W and 77° W from 76° W, 16°45′ S to 75°09′ W, 15°30′ S for concentrations of nitrate, nitrite, phosphate, silicate, turbidity and pH (right). For bottle data of the nutrient concentrations and pH the sampling depths are marked by black dots.

200 m depth salinity and temperature anomalies were positive and oxygen anomalies were slightly negative. Between 100 m and 200 m depth strong negative salinity, temperature and oxygen anomalies are present (Fig. 3). Distinct maxima of phosphate, silicate and nitrate concentration anomalies were located at 120 m to 150 m depth. Similar to near-shelf anticyclone A, turbidity was higher in the eddy between 50 m and 400 m, however, without the enhanced maximum below the mixed layer. The chlorophyll section shows a maximum of 2.5 (cc)µg L^{-1} in the core of the eddy (Fig. 4) at a 40 m depth in a layer of weak density stratification and is less than half as in the coastal anticyclone. As the mixed layer reached deeper, enhanced chlorophyll values reach down to about 80 m depth and hence deeper than for the coastal anticyclone A. The swirl velocity at 200 to 400 m depth was

southwest and the eddy signal was no longer visible, hence the time and location of formation could not be determined for eddy B. Nevertheless, eddy B was more than 5 months old and hence more than 3 months older than eddy A at the time of measurements.

3.4 The cyclonic feature (eddy C)

Table 1. Anomalies of mean anticyclonic (AE) and cyclonic (CE) eddies computed for the region 10° S to 20° S (Chaigneau et al., 2011) and for the 3 eddies A, B and C to a depth of 600 m although the vertical extent is even larger. Available heat anomaly (AHA) and available salt anomaly (ASA) within one eddy are computed following Chaigneau et al. (2011).

	Chaigneau et al. (2011)		A	B	C
	(AE)	(CE)	(AE)	(AE)	(CE)
Vertical extent (m)	0–450	0–200	0–600	0–600	0–600
Radius (km)	57.6	62.3	52.0	48.8	88.0
Volume ($\times 10^{12} m^3$)	4.9	2.6	5.2	4.7	14.8
AHA ($\times 10^{18}$J)	6.5	−5.9	17.7	3.7	−49.8
ASA ($\times 10^{10}$kg)	17.4	−14.7	36.5	18.7	−98.8

but no phytoplankton measurements were made during the cruise.

The chlorophyll concentrations of the subsurface maximum in eddy A are in the same concentration range as the chlorophyll concentrations in the surface layer of the coastal upwelling (see section A2 in Fig. 4). Assuming that chlorophyll concentrations can be taken as a (qualitative) indicator for primary productivity this finding suggests that eddies may play an important role for the overall productivity off Peru. Additionally, the development of a pronounced filament structure at the northern fringe of eddy A (which is clearly visible in the satellite picture, see Fig. 5) documents that due to the rotation of the eddy, highly productive surface waters are transported westward far beyond the narrow band of coastal upwelling at the shelf. However, there is large uncertainty involved with regard to biogeochemical significance of eddies given the small number of observations.

Both the vertical concentration distributions (Fig. 2), as well as the anomalies (Fig. 3) of oxygen and nutrients (i.e. nitrate, nitrite) in mode water eddy A reveal a core layer where pronounced loss of fixed nitrogen occurs. This is indicated by the pronounced maximum of NO_2^- concentrations (often also referred to as the secondary nitrite maximum, SNM) at about 250–300 m depth, which is associated with the pronounced minima of both O_2 ($< 5\,\mu mol\,L^{-1}$) and NO_3^- concentrations between 100 and 300 m depth. Please note that the OMZ (here defined as $O_2 < 20\,\mu mol\,L^{-1}$) spreads from 100 to 600 m depth. The co-occurrence of extremely depleted O_2 and NO_3^-, coinciding with high NO_2^- concentrations have been attributed to on-going denitrification (Fiadeiro and Strickland, 1968; Codispoti et al., 1986) or DNRA (Lam et al., 2009). Enhanced turbidity as a measure for suspended material and particles, is also found between 100 and 300 m in eddy A (Figs. 2 and 6) which indicates the existence of an intermediate nepheloid layer known to be associated with enhanced microbial activity. These layers are, moreover, known to play important roles in other OMZs adjacent to coastal upwelling regions such as the Arabian Sea and off NW Africa (Naqvi et al., 1993; Fischer et al., 2009).

A similar feature is seen in the O_2 and NO_2^-/NO_3^- distributions and anomalies (Figs. 3 and 7) of the mode water eddy B. The NO_3^- concentrations in the "aged" eddy B are, however, higher compared to the "young" eddy A. This apparent contradiction (the older an eddy the more NO_3^- should have been lost due to the ongoing N loss processes) is most probably resulting from higher initial NO_3^- concentrations at the time of formation of eddy B. The maximum concentration of NO_2^- of up to $5\,\mu mol\,L^{-1}$ measured in eddy B is significantly lower than that of up to $11\,\mu mol\,L^{-1}$ measured in eddy A. This points to a significantly lower activity of nitrogen loss processes in eddy B. The NO_2^- concentrations measured during our cruise in November 2012 are in the same range as those reported in previous studies of the SNM in the OMZ off Peru (see, for example, Barber and Huyer, 1979; Copin-

Chaigneau, A., Le Texier, M., Eldin, G., Grados, C., and Pizarro, O.: Vertical structure of mesoscale eddies in the eastern South Pacific Ocean: A composite analysis from altimetry and Argo profiling floats, J. Geophys. Res., 116, C11025, doi:10.1029/2011JC007134, 2011.

Chavez, F. P. and Messie, M.: A comparison of eastern upwelling boundary upwelling systems, Prog. Oceanogr., 83, 80–96, 2009.

Chelton, D. B., Schlax, M. G., Samelson, R. M., and de Szoeke, R. A.: Global observations of large oceanic eddies, Geophys. Res.

extraordinary mid-ocean plankton blooms, Science, 316, 1021–1026, 2007.

Morales, C. E., Hormazabel, S., Correa-Ramirez, M., Pizarro, O., Silva, N., Fernandez, C., Anabalon, V., and Torreblanco, M. L.: Mesoscale variability and nutrient-phytoplankton distribution off central-southern Chile during the upwelling season: The influence of mesoscale eddies, Prog. Oceanogr., 104, 17–29, 2012.

Naqvi, S. W. A., Dileep Kumar, M., Narvekar, P. V., De Sousa, S. N., George, M. D., and DeSilva, D.: An intermediate nepheloid layer associated with high microbial metabolic rates and denitrification in the northwestern Indian Ocean, J. Geophys. Res., 98, 16469–16479, 1993.

Oschlies, A. and Garcon, V.: Eddy-induced enhancement of primary production in a model of the North Atlantic Ocean, Nature, 394, 266–269, 1998.

Paulmier, A. and Ruiz-Pino, D.: Oxygen minimum zones (OMZs) in the modern ocean, Prog. Oceanogr., 80, 113–128, 2009.

Stramma, L., Johnson, G. C., Sprintall, J., and Mohrholz, V.: Expanding oxygen-minimum zones in the tropical oceans, Science,